PERGAMON

International Journal of Heat and Mass Transfer 44 (2001) 1517–1526

International Journal of HEAT and MASS TRANSFER

www.elsevier.com/locate/ijhmt

Dynamics of evaporating drops. Part I: formulation and evaporation model

Farzad Mashayek *

Department of Mechanical Engineering, University of Illinois at Chicago, 842 West Taylor Street, Chicago, IL 60607, USA

Received 24 August 1999; received in revised form 6 June 2000

Abstract

Modifications in the rate of evaporation of a drop due to its surface deformation are investigated using numerical simulations based on a Galerkin finite element method. It is first shown that, for a drop at its boiling temperature and surrounded by a gas at a uniform temperature (far from the drop surface), the liquid and the gas phases may be studied separately, provided a large density ratio. In this paper the results of the gas phase are presented. The surface of the drop is deformed using various spherical modes up to the eighth with amplitudes as large as 70% of the radius of the spherical drop. The mass transfer number is also varied from 0.1 to 2. The results show that the rate of evaporation increases with the increase of the amplitude of the surface deformation and varies significantly along the surface of the drop. A model has been extracted from the numerical results, which expresses the mass flux as a function of the surface curvature. The model is valid for surface amplitudes up to 10% of the drop radius.

1. Introduction

With the growing interest in analytical treatments of two-phase turbulent flows in recent years, there has been an associated increasing demand for analytical/empirical correlations describing the interphase transfer of mass, momentum, and energy [1–4]. As a result, a great deal of effort (e.g., [5–9]) has been devoted to numerically simulate the flow around a single (or a small ensemble of) drop(s). While previous studies have been very successful in providing new insights into the interactions between the two phases, they have been mostly concerned with "spherical" drops. However, a large number of two-phase systems involve liquid drops which undergo significant shape deformations while interacting with the carrier phase. The drop deformation could have significant effects on interphase transfer phenomenon, thus resulting in some modifications in the existing correlations.

Previous studies of deforming/evaporating drops are limited in both extent and scope of the contributions. This is, understandably, due to complexities involved in numerical modeling and detailed laboratory measurements of various phenomena present in the problem. From a numerical point of view, the main difficulty arises from the presence of a continuously evolving interface that is very closely coupled to the dynamics of the drop. One of the early studies is by Deng et al. [10] later reviewed by Jeng and Deng [11]. In this work, a two-dimensional numerical model has been developed for investigating the dynamics of nonevaporating and evaporating long cylindrical drops undergoing deformation/breakup, and oscillations under viscous convective flows. The results show that the dynamics of the drop deformation is basically unaffected by vaporization, however, the evaporation rates (per unit area) are greater for deformed drops. Haywood et al. [12,13] perform numerical simulations of both statically deformed and oscillating, axisymmetric evaporating drops exposed to a convective flow field. The numerical model is based on the finite volume method, using a nonorthogonal adaptive grid. Computations of the steady state evaporation of *n*-heptane droplets in

* Tel.: (312) 996-5317; fax: (312) 413-0447.
E-mail address: mashaye@uic.edu (F. Mashayek).

0017-9310/01/$ - see front matter
PII: S0017-9310(00)00199-X

Nomenclature

B	$C_{pg}(T_\infty - T_b)/L_v$ transfer number
C_p	specific heat
F_n	$(3n+2)/2[n(n+1)+2]$
h	spine function
H	outside radius of the computational domain for the gas phase
k	thermal conductivity coefficient
$\mathscr{K}$	drop surface curvature
L_v	latent heat of evaporation
$\dot{m}$	mass flux
$\dot{M}$	rate of total evaporated mass
n	mode of oscillation
$\mathbf{n}$	outward unit normal vector
N_i	shape function
p	pressure
P_n	Legendre polynomial of degree n
Pr_g	$\rho_g \nu_g C_{pg}/k_g$ gas Prandtl number
r	radial (cylindrical) coordinate
r_0	initial radius of the nonperturbed drop
R_n	volume correction factor
Re_ℓ	$(1/\nu_\ell)(\sigma r_0/\rho_\ell)^{1/2}$ liquid Reynolds number
t	time
T	temperature
$\mathbf{w}$	(u, v) velocity vector
z	axial coordinate

Greek symbols

β	nondimensional rate of evaporation
ϵ_n	surface disturbance amplitude for mode n
θ	nondimensional gas temperature
ν	kinematic viscosity
ρ	density
σ	surface tension coefficient
$\boldsymbol{\tau}$	stress tensor
Υ	parameter in penalty function formulation
ϕ	inclination angle from the drop axis
χ	nondimensional mass flux
ψ	$(\chi - \chi_{sp})/\chi_{sp}$

Subscripts

b	boiling condition
g	gas
ℓ	liquid
s	drop surface
sp	spherical drop
∞	gas condition far from the drop surface

Symbol

ϱ	nondimensional radius of the spherical drop

high-temperature air show deformed oblate shapes with major axes perpendicular to the mean flow direction. Using the numerical result, Haywood et al. [12] propose a new correlation for the drag coefficient of (steady) deformed vaporizing drops. Oscillating drops are strongly damped at frequencies within 25% of the theoretical natural frequency of Lamb [14]. Haywood et al. [13] show that circulation inside the drop is responsible for the strong damping and promotes the formation of prolate shapes for drops.

While these previous studies have been helpful in unraveling several interesting phenomena, they are mainly concerned with the evolution of a drop in a combustor environment where strong convective fields tend to dominate the drop dynamics. The main objective of the present study is to investigate "free" oscillations of evaporating drops and the modifications of the rate of evaporation associated with such oscillations. We will consider both evaporation of deformed drops and oscillations of evaporating drops. While each of these subjects may be considered as a separate study on its own rights, a simultaneous analysis of the two is imperative in order to realistically address the issue of mass transfer from the surface of a deformed drop.

The results of our investigation are presented in two papers: Part I (the present paper) and Part II [15]. We consider the evaporation of a drop surrounded by a gas which is at a uniform temperature far from the surface of the drop. The preheat period is not considered and the drop is assumed to be at the liquid boiling temperature. With these assumptions we are able to investigate the effects of all of the parameters involved in the problem while a wide range for the variation of each parameter is considered. In Part I, after presenting the general formulation, it is shown that under these conditions and for a large density ratio, the gas phase and the liquid phase may be studied separately. The coupling of the two phases is through an evaporation model which is derived from the study of the gas phase in Part I. In Part II, this model is implemented to study free oscillations of evaporating drops using both numerical and theoretical approaches. A discussion of the effects of oscillations on the rate of evaporation is also presented in Part II. In Section 2, we present the formulation and elaborate on the (de)coupling of the two phases. In Section 3, the results of the gas phase are discussed followed by conclusions in Section 4.

2. Formulation

The main objective of this work is to study the dynamics of an evaporating and oscillating drop surrounded by a gas at a temperature T_∞ in zero gravity (Fig. 1). Since we are considering interactions of the gas with only one single drop, it can be assumed that the

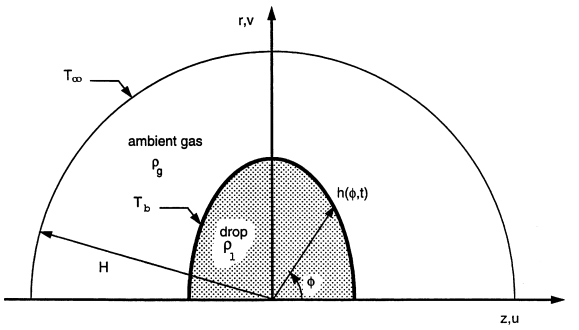

Fig. 1. Coordinate system and solution domain used in the computations.

total heat capacity of the gas much larger than that of the liquid and T_∞, far from the drop surface, is constant. Assuming that both the liquid and the gas are incompressible with constant properties, the conservation equations for mass, momentum, and energy are described as

$$\nabla \cdot \mathbf{w}_\alpha = 0, \tag{2.1}$$

$$\frac{\partial \mathbf{w}_\alpha}{\partial t} + \mathbf{w}_\alpha \cdot \nabla \mathbf{w}_\alpha = -\frac{1}{\rho_\alpha}\nabla p_\alpha + v_\alpha \nabla^2 \mathbf{w}_\alpha, \tag{2.2}$$

$$\frac{\partial T_\alpha}{\partial t} + \mathbf{w}_\alpha \cdot \nabla T_\alpha = \frac{k_\alpha}{\rho_\alpha C_{p\alpha}}\nabla^2 T_\alpha, \ \alpha = \ell, g, \tag{2.3}$$

where ℓ and g stand for liquid and gas, respectively.

For a liquid drop evaporating with a mass flux $\dot{m}$, the jump condition and the normal stress balance on the interface are, respectively, described as [16,17]

$$\dot{m} = \rho_\ell(\mathbf{w}_\ell - \mathbf{w}_s)\cdot\mathbf{n} = \rho_g(\mathbf{w}_g - \mathbf{w}_s)\cdot\mathbf{n}, \tag{2.4}$$

$$\dot{m}(\mathbf{w}_g - \mathbf{w}_\ell)\cdot\mathbf{n} + [\mathbf{n}\cdot(\boldsymbol{\tau}_g - \boldsymbol{\tau}_\ell)]\cdot\mathbf{n} + \sigma\nabla\cdot\mathbf{n} = 0, \tag{2.5}$$

where $\boldsymbol{\tau}$ is the stress tensor including the pressure component. The first term on the left-hand side of (2.5) is the so-called "recoil force" which is a result of the change in the momentum of the liquid during vaporization. In this study, we assume that the drop is at the liquid boiling temperature, T_b. In many problems the transient heating period does not significantly affect the droplet lifetime, and more rigorous calculations for spherical drops show that the droplet surface temperature is only slightly less than the liquid boiling point in combustion environments. This assumption eliminates the need to solve the energy equation in the liquid phase as well as the need to solve the vapor transport (species) equation ([18], p. 309). This also eliminates the possibility for formation of thermocapillary flows due to the variations of surface tension with temperature. With this assumption, the energy received by the drop is consumed for phase change only, and the following equation can be stated for the balance of energy at the surface of the drop:

$$\dot{m}L_v = k_g \nabla T_g \cdot \mathbf{n}. \tag{2.6}$$

The governing equations of the two phases are coupled through the interface relations (2.4)–(2.6) and must be solved simultaneously. However, we show in the following that the coupling of the two phases can be removed for the cases considered in this study – note that this decoupling must be applicable to oscillating drops. The starting point is to eliminate $\mathbf{w}_s$ in (2.4) to obtain

$$(\mathbf{w}_g - \mathbf{w}_\ell)\cdot\mathbf{n} = \frac{\dot{m}}{\rho_g}\left(1 - \frac{\rho_g}{\rho_\ell}\right). \tag{2.7}$$

We then simplify (2.5) by noting that the fluid pressure affects the oscillations of the drop through its fluctuating component which is proportional to the fluid's density (see e.g., [14] for nonevaporating drops). In this study, we consider $\rho_g \ll \rho_\ell$, therefore, the effects of the fluctuations in the ambient gas pressure may be neglected in comparison to the effects of the pressure fluctuations in the liquid. Further, the mean pressure of the gas affects only the mean pressure of the drop and, for incompressible liquid, does not influence the oscillations of the drop – in Part II we show that the effect of the ambient gas pressure on the period of oscillations of an inviscid, evaporating drop is proportional to ρ_g/ρ_ℓ. We also note that the viscosity of the gas is much smaller than that of the liquid. As a result, $\boldsymbol{\tau}_g$ can be eliminated from (2.5) which, by implementing (2.7), yields

$$\mathbf{n}\cdot\boldsymbol{\tau}_\ell\cdot\mathbf{n} = \sigma\nabla\cdot\mathbf{n} + \frac{\dot{m}^2}{\rho_g}. \tag{2.8}$$

In this manner, the mean pressure of the drop is calculated relative to the mean pressure of the ambient gas. Finally, (2.7) can be further simplified by noting that the ratio of the velocity of the liquid to that of the gas, at the interface, is of the same order as ρ_g/ρ_ℓ. Therefore, (2.7) may be approximated as

$$\mathbf{w}_g\cdot\mathbf{n} = \frac{\dot{m}}{\rho_g}. \tag{2.9}$$

With these simplifications, the coupling between the two phases is now through the evaporated mass, $\dot{m}$, only. In order to eliminate this coupling, we assume that the time scale for changes in the velocity and temperature of the gas is small compared to the time scale of the evolution of the surface of the oscillating drop (we will elaborate on the validity of this assumption in Section 3.1). Therefore, the gas phase may be considered quasi-steady during the evolution of the drop surface. A study of quasi-steady evaporation of deformed drops is presented in Section 3 where we demonstrate that the flux of evaporated mass can be modeled as a function of the

local surface curvature. The evaporation model produced by the quasi-steady analysis is then implemented for the investigation of drop oscillations in Part II.

The governing equations for both phases are nondimensionalized using the initial radius of the nonperturbed spherical drop, r_0, a characteristic time, $(\rho_\ell r_0^3/\sigma)^{1/2}$, and a normalized gas temperature $\theta = (T_g - T_b)/(T_\infty - T_b)$

$$\nabla \cdot \mathbf{u}_\alpha = 0, \qquad \alpha = \ell, g \tag{2.10}$$

$$\frac{D^\alpha \mathbf{u}_\alpha}{Dt} = \frac{v_\alpha}{v_\ell}\frac{1}{Re_\ell}\nabla \cdot \mathbf{T}_\alpha, \qquad \alpha = \ell, g \tag{2.11}$$

$$\frac{D^g \theta}{Dt} = \frac{v_g}{v_\ell}\frac{1}{Re_\ell Pr_g}\nabla^2\theta, \tag{2.12}$$

where $\mathbf{T}_\alpha = -p_\alpha \mathbf{I} + [\nabla \mathbf{u}_\alpha + (\nabla \mathbf{u}_\alpha)^T]$ for Newtonian fluid with p_α now denoting the normalized pressure, and $\frac{D^\alpha}{Dt} = \frac{\partial}{\partial t} + \mathbf{u}_\alpha \cdot \nabla$ is the total derivative operator. Here, $Re_\ell = (1/v_\ell)(\sigma r_0/\rho_\ell)^{1/2}$ is the Reynolds number based on the liquid properties and $Pr_g = \rho_g v_g C_{pg}/k_g$ is the gas Prandtl number. Note that no energy equation is considered for the liquid phase as the drop is assumed to be at its boiling temperature. Boundary conditions for each phase are discussed later.

2.1. Methodology

The governing equations are solved in (r, z) coordinates using a Galerkin finite element method with penalty function formulation [19]. Here, the pressure is eliminated from the set of unknown variables by absorbing the continuity equation into the momentum equation. For that, the pressure is defined as

$$p_\alpha = -\Upsilon \nabla \cdot \mathbf{u}_\alpha, \tag{2.13}$$

where Υ is a large number [$\mathcal{O}(10^9)$] depending on the viscosity and Reynolds number. Four-node bilinear isoparametric elements are used to approximate the velocity distribution over each element

$$\mathbf{u}_\alpha(z, r, t) = \sum_{i=1}^{4} \mathbf{u}_{\alpha i}(t) N_i(z, r). \tag{2.14}$$

$$\theta(z, r, t) = \sum_{i=1}^{4} \theta_i(t) N_i(z, r). \tag{2.15}$$

To obtain the finite element formulation, the momentum and energy equations are multiplied by the shape function, N_j, and integration is carried over the element volume. After the divergence theorem is invoked the following closed form finite element formulation is obtained:

$$\int_\Omega \left(\frac{v_\ell}{v_\alpha} Re_\ell N_j \frac{D^\alpha \mathbf{u}_\alpha}{Dt} + \nabla N_j^T \cdot \left[\Upsilon(\nabla \cdot \mathbf{u}_\alpha)\mathbf{I} + [\nabla \mathbf{u}_\alpha + (\nabla \mathbf{u}_\alpha)^T] \right] \right) d\Omega = \int_\xi N_j \mathbf{T}_\alpha \cdot \mathbf{n}\, d\xi, \tag{2.16}$$

$$\int_\Omega \left(\frac{v_\ell}{v_g} Re_\ell Pr_g N_j \frac{D^g \theta}{Dt} + \nabla N_j \cdot \nabla \theta \right) d\Omega = \int_\xi N_j \nabla \theta \cdot \mathbf{n}\, d\xi, \tag{2.17}$$

where Ω and ξ indicate the volume and the surface of the element, respectively.

3. Evaporation of deformed drops

In this section, the solution of Eqs. (2.10)–(2.12), with $\alpha = g$, is sought for the gas phase. The solution domain, shown in Fig. 1, extends from the surface of the drop to a distance H where the gas temperature can be considered uniform at T_∞. The boundary conditions for the velocity field are obtained using (2.6) and (2.9) on the surface of the drop

$$u_g = \frac{v_g}{v_\ell}\frac{B}{Re_\ell Pr_g}\frac{\partial \theta}{\partial z}, \quad v_g = \frac{v_g}{v_\ell}\frac{B}{Re_\ell Pr_g}\frac{\partial \theta}{\partial r}, \quad \theta = 0, \tag{3.1}$$

and using conservation of mass at a distance H from the center of the drop

$$u_g = \frac{\dot{M}}{4\pi H^2}\cos\phi, \quad v_g = \frac{\dot{M}}{4\pi H^2}\sin\phi, \quad \theta = 1. \tag{3.2}$$

Here, $B = C_{pg}(T_\infty - T_b)/L_v$ is the transfer number, and $\dot{M}$ represents the total mass evaporated from the surface of the drop per unit time. We consider axisymmetric drops for which symmetry boundary conditions are used along the symmetry axis

$$\frac{\partial u_g}{\partial r} = 0, \quad v_g = 0, \quad \frac{\partial \theta}{\partial r} = 0 \text{ at } r = 0. \tag{3.3}$$

For cases that the surface of the drop is deformed with even spherical modes (see below), symmetry boundary conditions are also implemented on the plane of symmetry

$$u_g = 0, \quad \frac{\partial v_g}{\partial z} = 0, \quad \frac{\partial \theta}{\partial z} = 0 \text{ at } z = 0. \tag{3.4}$$

The surface of the drop, $h(\phi)$, is perturbed from its spherical shape using spherical harmonics

$$h(\phi) = R_n[1 + \epsilon_n P_n(\cos\phi)], \tag{3.5}$$

where $P_n(\cos\phi)$ is the Legendre polynomial of degree n, ϵ_n the amplitude of the disturbance, and R_n is used to

maintain the volume of the drop constant when ϵ_n is varied

$$R_2 = \left(\frac{35}{35+21\epsilon_2^2+2\epsilon_2^3}\right)^{1/3},$$
$$R_3 = \left(\frac{7}{7+3\epsilon_3^2}\right)^{1/3},$$
$$R_4 = \left(\frac{3003}{3003+1001\epsilon_4^2+54\epsilon_4^3}\right)^{1/3}, \quad (3.6)$$
$$R_5 = \left(\frac{11}{11+3\epsilon_5^2}\right)^{1/3}.$$

An inspection of the formulation reveals that v_g/v_ℓ and Re_ℓ only affect the time scale and do not change the long time values of evaporation rate. Since we are interested in the steady state solution, in the following we will only consider the effects of B, n, and ϵ_n. For all the simulations, we use $Pr_g = 1$ which is a good approximation for most gases. To expedite the convergence, the initial condition for each simulation is taken from the analytical solution for quasi-steady evaporation of a spherical drop at the same B. For each value of B, the numerical solution is first confirmed by comparison of the results obtained for a nonperturbed drop with the analytical solution for evaporation of a spherical drop [18]

$$\chi_{sp} = \frac{2}{\varrho}\beta, \quad (3.7)$$

where subscript 'sp' refers to spherical drop with non-dimensional radius ϱ, and

$$\chi = \left(\frac{\rho_\ell \sigma}{r_0}\right)^{-1/2}\dot{m},$$
$$\beta = \frac{1}{2}(\rho_\ell r_0 \sigma)^{-1/2}\left(\frac{k_g}{C_{pg}}\right)\ln(1+B). \quad (3.8)$$

The value of H for each simulation is chosen such that boundary conditions (3.2) are satisfied while the tangential velocity (v_ϕ) and the temperature gradient become sufficiently close to zero at distance H. The average value used for various cases is approximately $H = 90$. Typically, 60 (uniform) and 20 (stretched) elements were used in the circumferential and radial directions, respectively, for even-mode cases.

Of particular interest in this work, is the variation of the vapor mass flux along the surface of the drop. Fig. 2 shows the parameter

$$\psi = \frac{\chi - \chi_{sp}}{\chi_{sp}}, \quad (3.9)$$

as a function of angle ϕ at different surface amplitudes for $B = 1$ and $n = 2$, 3, and 4. The parameter ψ measures the deviation of the mass flux of the deformed drop from

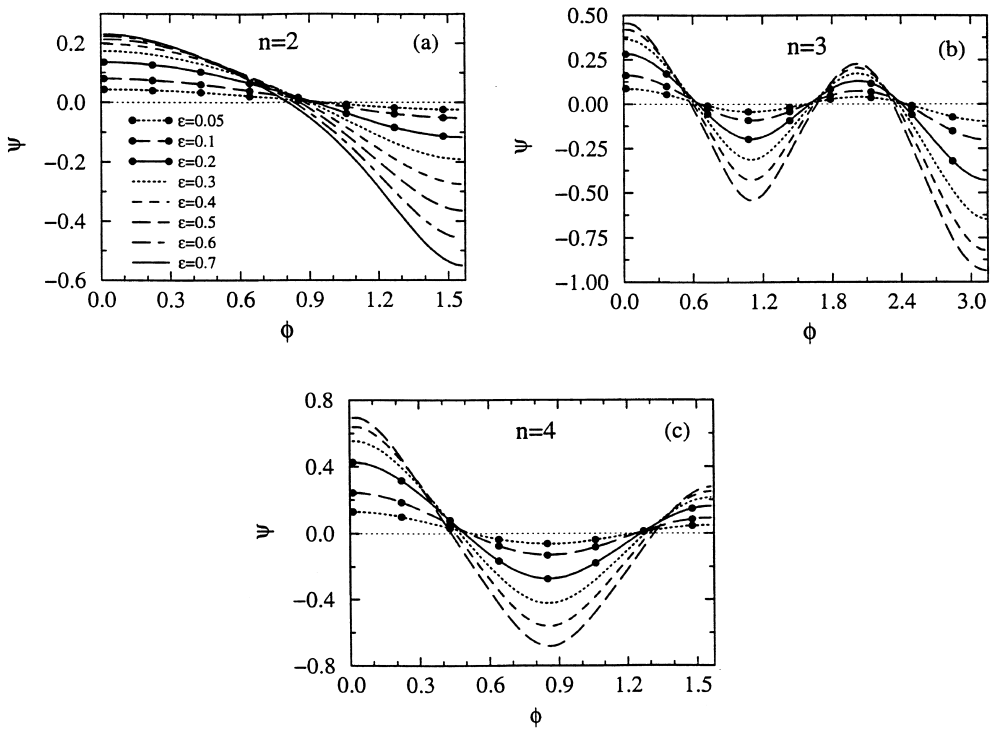

Fig. 2. Variations of the normalized mass flux with angle ϕ at various amplitudes for (a) $n = 2$, (b) $n = 3$, and (c) $n = 4$.

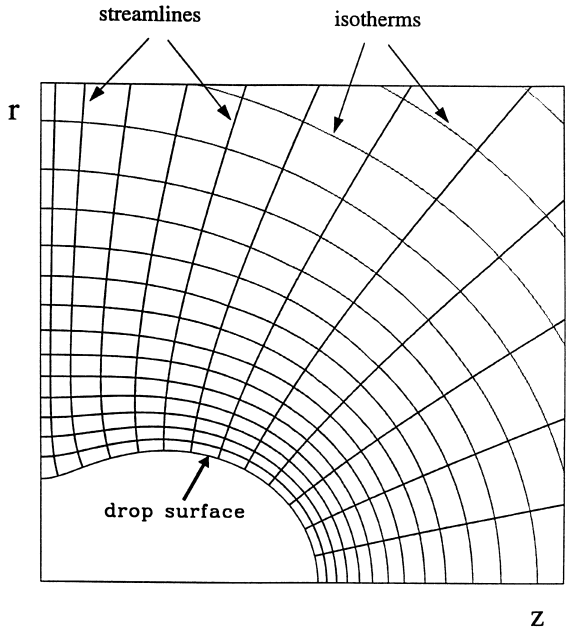

Fig. 3. Isotherms and streamlines near the surface of the drop for a case with $\epsilon_2 = 0.7$ and $B = 1$.

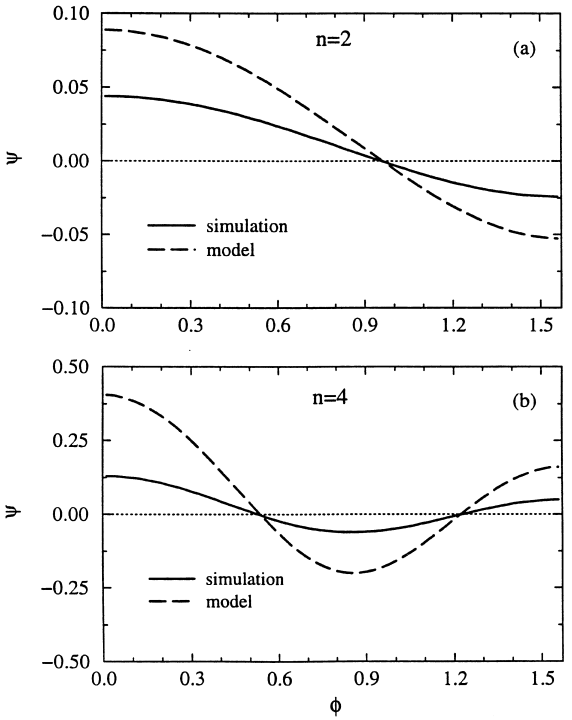

Fig. 4. Comparison between the simulation results and predictions of a preliminary model for the normalized mass flux as a function of ϕ for (a) $n = 2$ and (b) $n = 4$.

that of a spherical drop. It is observed that the local values of ψ can be very significant indicating changes in the mass flux as large as 70% (for $\epsilon_4 = 0.5$). While the change in the total evaporated mass (for the same case) is only 9%, the large local variations of the mass flux can have significant effects on the oscillations of an evaporating drop. In general, the magnitude of ψ increases with the increase of the amplitude of the surface deformation. However, it appears that the rate of increase of the magnitude of ψ with ϵ is larger near the plane of symmetry ($\phi = \pi$). The variation of ψ with ϕ can be explained by examining the isotherms near the surface of the drop, as shown in Fig. 3, for a drop deformed in second mode with $\epsilon_2 = 0.7$. It is noted that the normal distance between the isotherms varies with angle ϕ. In particular, for this second-mode case, the isotherms are more apart near $\phi = \pi$ and result in the decrease of the mass flux with respect to that of a spherical drop. The variation of streamlines near the surface of the drop is also shown in Fig. 3. The streamlines are formed perpendicularly to the isotherms and tend to align radially away from the surface of the drop.

3.1. Evaporation model for small amplitudes

In the absence of a model for evaporation of deformed surfaces, Lian and Reitz [20] use a modified form of (3.7) to study the instability of evaporating liquid jets. They postulate that the deformed surface may be locally considered as the surface of a spherical drop having the same curvature, $\mathscr{K}$, as that of the deformed surface. Therefore, $\chi = \mathscr{K}\beta$ is used which for $\mathscr{K} = 2/\varrho$ reduces to (3.7) for a spherical drop. The results of our numerical simulations presented in the form of variations of the normalized mass flux, ψ, with ϕ in Fig. 2 also suggest a correlation between the mass flux and the local surface curvature of the deformed drop.

Figure 4 shows a comparison between $\psi_{\text{sim}} = (\chi - \chi_{\text{sp}})/\chi_{\text{sp}}$ from the simulation results and $\psi_{\text{mod}} = (\mathscr{K}\beta - \chi_{\text{sp}})/\chi_{\text{sp}}$ based on the model discussed above for $n = 2$ and 4, with $B = 1$ and $\epsilon = 0.05$. Here, the local curvature of the surface is calculated numerically using

$$\mathscr{K} = -\frac{h^2 + 2h_\phi^2 - hh_{\phi\phi}}{(h_\phi^2 + h^2)^{1.5}} - \frac{h - \cot\phi h_\phi}{h(h_\phi^2 + h^2)^{0.5}}, \tag{3.10}$$

where subscript shows derivative with respect to ϕ. Although large deviations are observed, the comparison in Fig. 4 does suggest that a good agreement can be achieved by implementing a coefficient F_n (independent of ϕ) such that: $\psi_{\text{sim}} = F_n\psi_{\text{mod}}$. Then, substituting for ψ_{sim} and ψ_{mod}, and solving for the mass flux χ, it is easy to show that

$$\chi = \left[F_n\left(\mathscr{K} - \frac{2}{\varrho}\right) + \frac{2}{\varrho}\right]\beta. \tag{3.11}$$

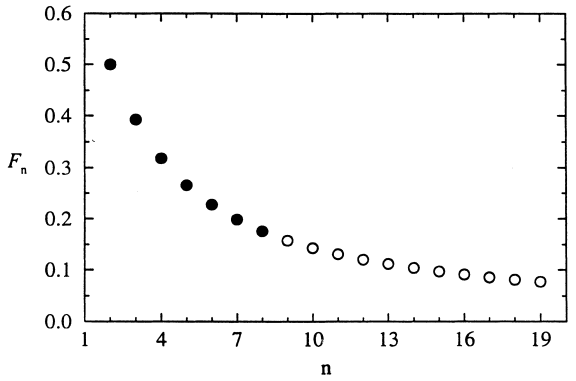

Fig. 5. Variations of the coefficient F_n with the mode of surface deformation. The solid symbols correspond to the cases simulated and the hollow symbols show extrapolated values.

A comparison between Figs. 4(a) and (b) shows that the coefficient F_n depends on the mode of oscillation n. By inspection, we have managed to compile our simulation results for the first few modes into the following relation for F_n:

$$F_n = \frac{3n+2}{2[n(n+1)+2]}. \tag{3.12}$$

The discrete values of F_n are plotted in Fig. 5 versus mode of oscillation. The solid symbols indicate the modes of oscillations that have been simulated in this study. The hollow symbols show the extrapolation of F_n based on (3.12). The largest value, $F_n = 0.5$, belongs to the second mode and F_n decreases monotonically with the increase of n.

In order to assess the evaporation model (3.11), a variety of cases have been simulated for $\epsilon = 0.05$. The results of these simulations are presented in Figs. 6 (for $n = 2$, 3, 4, and 5) and 7 (for $n = 6$, 7, and 8) for $B = 0.1$, 0.5, 1, and 2. It must be mentioned that no volume correction factor (R_n, Eq. (3.6)) has been used for cases shown in Fig. 7. However, this does not have any significant effect on ψ as R_n becomes very close to unity for higher modes at $\epsilon = 0.05$. It is clearly observed in Figs. 6 and 7 that ψ may be considered independent of B and that the model is capable of predicting the variations of ψ with ϕ accurately. It is also interesting to note that the agreement between the model prediction and simulation results does not diminish with the

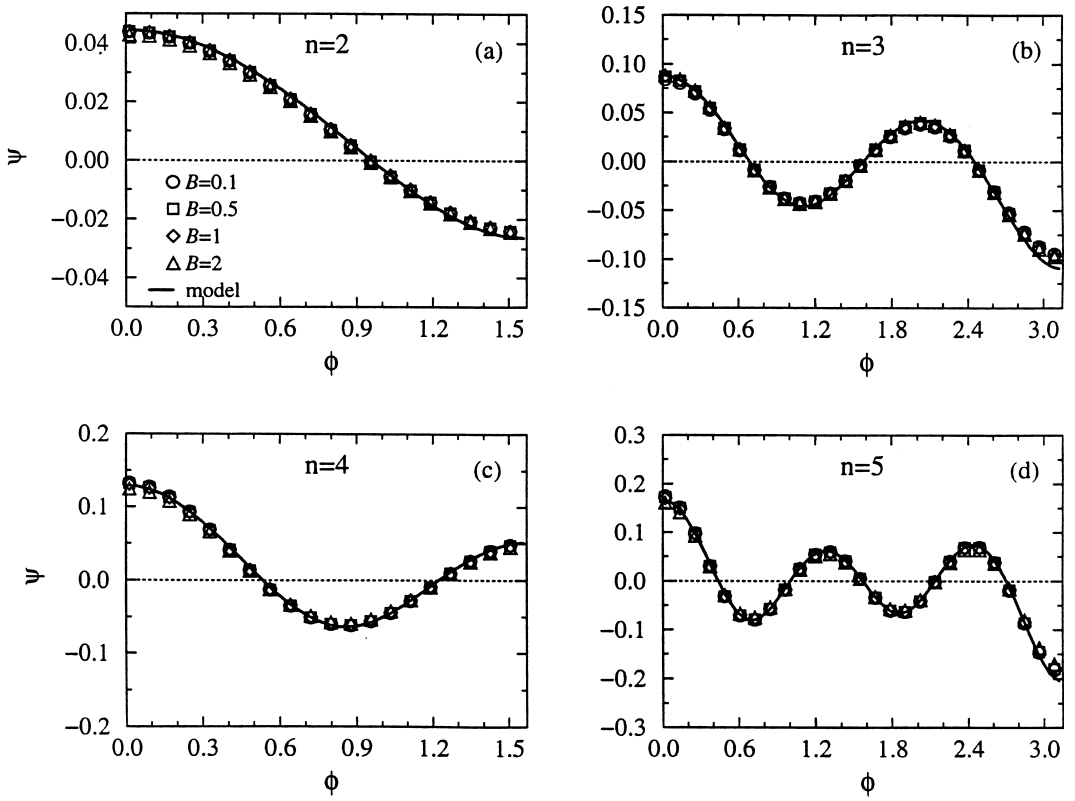

Fig. 6. Comparison between the model prediction and simulation results for the normalized mass flux at different values of B. (a) $n = 2$, (b) $n = 3$, (c) $n = 4$, and (d) $n = 5$.

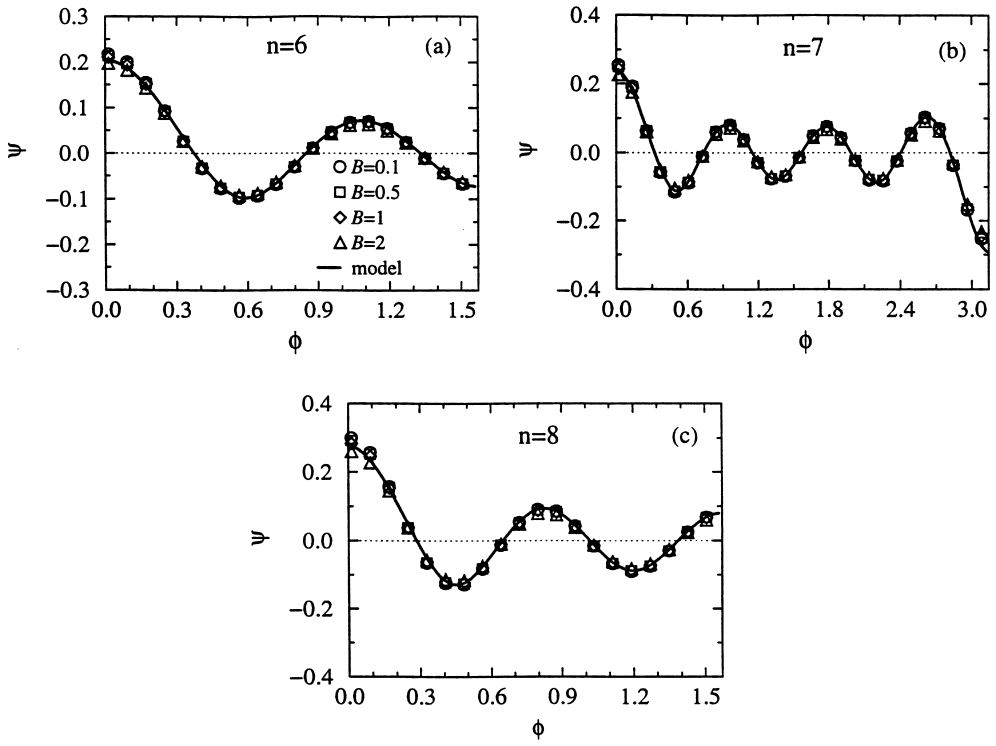

Fig. 7. Comparison between the model prediction and simulation results for the normalized mass flux at different values of B. (a) $n = 6$, (b) $n = 7$, and (c) $n = 8$.

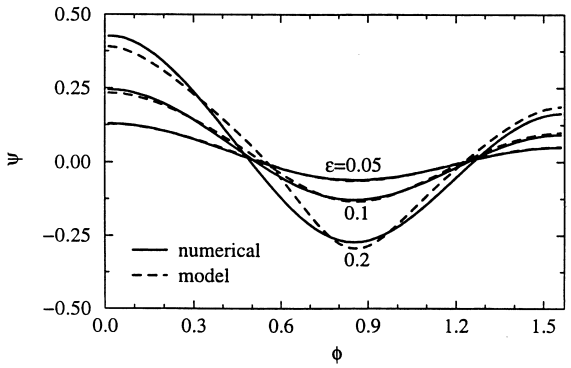

Fig. 8. Comparison between the model prediction and simulation results at $B = 1$ for a fourth-mode surface deformation at various amplitudes.

increase of the mode of oscillation. Therefore, although the performance of the model has not been assessed for $n > 8$, we feel that higher modes could also be well represented by (3.11).

More inspection of the results indicates that an important parameter affecting the performance of the model is the amplitude of the surface deformation. In Fig. 8 comparisons are provided between the model prediction and simulation results for ψ at three different amplitudes $\epsilon_4 = 0.05$, 0.1, and 0.2. The figure suggests that the model performance deteriorates with the increase of the amplitude, however, a reasonable agreement is observed for up to $\epsilon_4 = 0.1$. The results for other modes (not shown) also indicate a similar trend. In the study of oscillations of drops in Part II, we will only consider $\epsilon = 0.05$ for which the model describes the local rate of evaporation accurately.

It was argued in Section 2 that the study of the gas phase could be decoupled from the effects of the liquid phase provided that the evolution of the velocity and temperature fields of the gas phase is fast compared to the motion of the drop surface. In order to provide an assessment of the validity of this assumption, we consider the transient behavior of the gas phase. It is not possible to exactly create the same transient conditions as those in the real oscillating drop. However, as a reasonable approximation for a drop oscillating in fourth mode with initial amplitude of 0.05, we perturb the surface of the drop with $\epsilon_4 = 0.05$ and plot the evolution of ψ in time in Fig. 9. The initial conditions for velocity and temperature in this transient problem are taken from the numerical simulation for a spherical drop at the same transfer number $B = 1$. Fig. 9 shows that the solution at $t = 0.06$ closely approximates the steady state

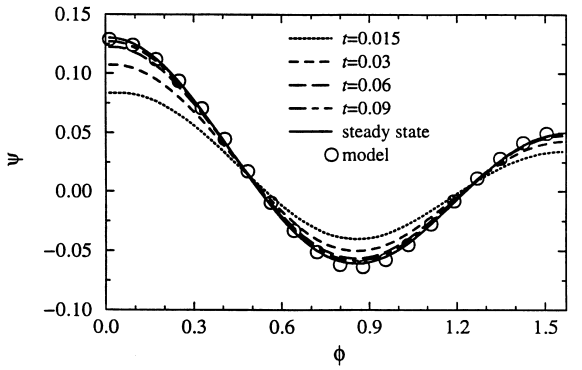

Fig. 9. Temporal evolution of the normalized mass flux for a case with $\epsilon_4 = 0.05$ and $B = 1$.

solution. This time is to be compared to ~ 0.19 (see Part II) which is the time required to change the amplitude of oscillation by 0.05 in the fourth mode oscillation of a drop with $\epsilon = 0.05$. Although this simulation does not exactly replicate the conditions in the oscillating drop, it does provide some support for the assumption of quasi-steadiness. More importantly, Fig. 9 shows that the variation of ψ with ϕ is similar for different times. Therefore, the transient solution of ψ at various times may be related to its steady state solution by applying a coefficient similar to F_n. Consequently, the model presented in this section is capable of representing the transient behavior by applying a modification to F_n.

4. Conclusion

Numerical simulations are used to investigate the modifications in the rate of evaporation of a drop due to its surface deformation. The preheat period is not considered and the drop is assumed to be at its boiling temperature. The surrounding gas, except for the region close to the drop, is also at a uniform temperature and its density is much smaller than the liquid density. Under these assumptions, it is shown that the gas and the liquid phases can be studied separately. The coupling between the two phases is through an evaporation model which is derived from the study of the gas phase and is then implemented to analyze the oscillations in the liquid phase.

In the analysis of the gas phase, the numerical solution to the steady state Navier–Stokes and energy equations is sought. The surface of the drop is perturbed with various spherical modes up to the eighth, the amplitude of disturbance is varied from small values up to 0.7, and a wide range of variation is considered for the transfer number. The results show that the mass flux varies along the surface of the deformed drop, due to modifications of the isotherms near the interface. The results for various transfer numbers become nearly identical when the modifications in the mass flux for each transfer number are normalized with the mass flux of the respective spherical drop (cf. Figs. 6 and 7). The variations of the mass flux, for small amplitudes, have been modeled as a function of surface curvature. The model is valid for surface amplitudes up to 10% of the radius of the drop and agrees very well with numerical results for spherical modes $n = 2$ to 8.

Acknowledgements

The support for this work was provided by the National Science Foundation under Grant CTS-9874655 with Dr. M.C. Roco as Program Director and by the US Office of Naval Research under Grant N00014-99-1-0808 with Dr. G.D. Roy as Technical Monitor.

References

[1] G.M. Faeth, Mixing, transport and combustion in sprays, Prog. Energy Combust. Sci. 13 (1987) 293–345.
[2] F. Mashayek, Droplet-turbulence interactions in low-mach-number homogeneous shear two-phase flows, J. Fluid Mech. 376 (1998) 163–203.
[3] F. Mashayek, Numerical investigation of reacting droplets in homogeneous shear turbulence, J. Fluid Mech. 405 (2000) 1–36.
[4] R.S. Miller, J. Bellan, Direct numerical simulation of a confined three-dimensional gas mixing layer with one evaporating hydrocarbon-droplet laden stream, J. Fluid Mech. 384 (1999) 293–338.
[5] G. Patnaik, A numerical solution of droplet vaporization with convection, Ph.D. Thesis, Carnegie-Mellon University, Pittsburgh, PA, 1986.
[6] J.M. Conner, S.E. Elghobashi, Numerical solution of laminar flow past a sphere with surface mass transfer, Numer. Heat Transfer 12 (1987) 57–82.
[7] C.H. Chiang, W.A. Sirignano, Axisymmetric calculations of three-droplet interactions, Atomization Sprays 3 (1) (1991) 91–108.
[8] I. Kim, S. Elghobashi, W.A. Sirignano, Three-dimensional flow over two spheres placed side by side, J. Fluid Mech. 246 (1993) 465–488.
[9] I. Kim, S. Elghobashi, W.A. Sirignano, Unsteady flow interactions between an advected cylindrical vortex tube and a spherical particle, J. Fluid Mech. 288 (1995) 123–155.
[10] Z.T. Deng, R.J. Litchford, S.M. Jeng, Two-dimensional simulation of droplet evaporation at high pressure, AIAA Paper 29-3122, 1992.
[11] S.M. Jeng, Z. Deng, Numerical simulation of deformed droplet dynamics and evaporation, in: K.K. Kou (Ed.), Recent Advances in Spray Combustion: Spray Combustion Measurements and Model Simulation, Volume II, Progress in Astronautics and Aeronautics, Vol. 171, AIAA Publishing Co., Reston, VA, 1996, pp. 305–328 (Chapter 12).

[12] R.J. Haywood, M. Renksizbulut, G.D. Raithby, Numerical solution of deforming evaporating droplets at intermediate Reynolds numbers, Numer. Heat Transfer 26 (1994) 253–272.
[13] R.J. Haywood, M. Renksizbulut, G.D. Raithby, Transient deformation and evaporation of droplets at intermediate Reynolds numbers, Int. J. Heat Mass Transfer 37 (9) (1994) 1401–1409.
[14] H. Lamb, Hydrodynamics, sixth ed., Cambridge University Press, Cambridge, 1932.
[15] F. Mashayek, Dynamics of evaporating drops. Part II: free oscillations, Int. J. Heat Mass Transfer 44 (2001) 1527–1541.
[16] A. Prosperetti, M.S. Plesset, The stability of an evaporating liquid surface, Phys. Fluids 27 (1984) 1590–1603.
[17] F.J. Higuera, The hydrodynamic stability of an evaporating liquid, Phys. Fluids 30 (1987) 679–693.
[18] S.R. Turns, An Introduction to Combustion: Concepts and Applications, McGraw-Hill, New York, 1996.
[19] T. Hughes, W. Liu, A. Brooks, Finite element analysis of incompressible viscous flows by the penalty function formulation, J. Comput. Phys. 30 (1979) 1–60.
[20] Z.W. Lian, R.D. Reitz, The effect of vaporization and gas compressibility on liquid jet atomization, Atomization Sprays 3 (3) (1993) 249–264.